Mon. Not. R. Astron. Soc. **000**, 1–17 (2013) Printed 6 October 2015 (MN LATEX style file v2.2)

Formation of In Situ Stellar Haloes in Milky Way-Mass Galaxies

Andrew P. Cooper[1⋆], Owen H. Parry[2], Ben Lowing[1], Shaun Cole[1] and Carlos Frenk[1]
[1]*Institute for Computational Cosmology, Department of Physics, University of Durham, South Road, Durham, DH1 3LE, UK*
[2]*Department of Astronomy, University of Maryland, College Park, MD 20742, USA*

Accepted 2015 September 03. Received 2015 August 11; in original form 2015 January 21

ABSTRACT

We study the formation of stellar haloes in three Milky Way-mass galaxies using cosmological smoothed particle hydrodynamics simulations, focusing on the subset of halo stars that form *in situ*, as opposed to those accreted from satellites. *In situ* stars in our simulations dominate the stellar halo out to 20 kpc and account for 30-40 per cent of its total mass. We separate *in situ* halo stars into three straightforward, physically distinct categories according to their origin: stars scattered from the disc of the main galaxy ('heated disc'), stars formed from gas smoothly accreted on to the halo ('smooth' gas) and stars formed in streams of gas stripped from infalling satellites ('stripped' gas). We find that most belong to the stripped gas category. Those originating in smooth gas outside the disc tend to form at the same time and place as the stripped-gas population, suggesting that their formation is associated with the same gas-rich accretion events. The scattered disc star contribution is negligible overall but significant in the Solar neighbourhood, where $\gtrsim$ 90 per cent of stars on eccentric orbits once belonged to the disc. However, the distinction between halo and thick disc in this region is highly ambiguous. The chemical and kinematic properties of the different components are very similar at the present day, but the global properties of the *in situ* halo differ substantially between the three galaxies in our study. In our simulations, the hierarchical buildup of structure is the driving force behind not only the accreted stellar halo, but also those halo stars formed *in situ*.

Key words: methods: numerical – galaxies:formation – galaxies: haloes– galaxies: structure

1 INTRODUCTION

Following Searle & Zinn (1978), much observational and theoretical work on the Milky Way's stellar halo has focused on the tidal stripping and disruption of satellite galaxies. The idea that galactic stellar haloes are built mainly by accretion is well supported by theoretical predictions of the standard dark energy/cold DM (ΛCDM) cosmogony (White & Frenk 1991; Bullock & Johnston 2005; Cooper et al. 2010) and direct evidence of tidal streams around nearby galaxies (Belokurov et al. 2006; McConnachie et al. 2009; Martínez-Delgado et al. 2010). However, recent work has shown that some aspects of the Milky Way's stellar halo may be difficult to explain by accretion alone, notably its central concentration and uniformity across the sky (Carollo et al. 2007; Bell et al. 2008; Cooper et al. 2011; **?**; Deason et al. 2011; Helmi et al. 2011; Xue et al. 2011).

Meanwhile, hydrodynamical simulations have predicted a distinct '*in situ*' halo component, defined (loosely) as having formed bound to the Milky Way itself rather than to any of its hierarchical progenitors (Abadi et al. 2003; Brook et al. 2004; Zolotov et al. 2009; Font et al. 2011; Tissera et al. 2013; Pillepich et al. 2015). Such haloes are a natural outcome of the ΛCDM model, which predicts that the vast majority of stars in a galaxy like the Milky Way form from the cooling of gas trapped by the galaxy's own DM (DM) potential (White & Rees 1978; White & Frenk 1991). The bulk of these *in situ* stars can be identified with the kinematically cold, rapidly rotating Galactic disc, but the proto-Milky Way may also have suffered strong perturbations from satellites and quasi-secular rearrangement (e.g. 'disc flips'; Bett & Frenk 2012), or even wholesale destruction and regrowth before the majority of present-day disc stars were formed (e.g. Sales et al. 2012; Aumer & White 2013; Aumer et al. 2013). If real galaxies pass through such messy stages of formation, it seems likely that a significant fraction of stars formed in the early Galaxy would now have highly eccentric orbits.

⋆ E-mail: a.p.cooper@durham.ac.uk

Recent simulations find that these *in situ* processes create haloes that are more concentrated, metal-rich and oblate than those formed by accreted stars (McCarthy et al. 2012). This supports the hypothesis of a transition between an *in situ* and an accreted halo as an explanation for the apparently 'bimodal' properties of halo stars observed in the Milky Way (Carollo et al. 2010; Beers et al. 2012; Tissera et al. 2014).

However, quantitative results concerning the origin of *in situ* halo stars and their importance relative to accreted stars are still very uncertain. Where they rely on simulations, such conclusions can be particularly sensitive to the numerical methods used. Starting from identical initial conditions, current state-of-the-art simulations predict substantially different properties for the bulk of the *in situ* stellar mass in Milky Way-like DM haloes (e.g. Scannapieco et al. 2012; Aumer et al. 2013), not just the few per cent that might be identified with an *in situ* halo. Moreover, the properties of *in situ* haloes may be much more sensitive to certain modelling choices than those of massive stellar discs, including prescriptions for star formation and the treatment of the multi-phase interstellar medium (ISM; for example, the mixing of hot and cold in galactic winds, tidal streams and cold clumps of free-falling gas).

Here we analyse the origin of *in situ* halo stars using three Milky Way-scale simulations run with the code described in Parry et al. (2012), one of the participants in the Aquila comparison project (Scannapieco et al. 2012). Two of the three DM haloes we simulate have also been simulated by Tissera et al. (2012, hearafter T12) and Tissera et al. (2013, 2014, hearafter T13, T14) using different 'subgrid' recipes for star formation and feedback but an otherwise similar hydrodynamic solver and identical initial conditions. We define what we mean by *in situ* halo stars in a straightforward and easily reproducible way. Careful definitions are particularly important for this problem because the concept of an *in situ* halo straddles an extremely fuzzy boundary between all the conventional Galactic components – disc, thick disc, bulge and halo. Based on these definitions, we discuss physical mechanisms by which *in situ* haloes are generated in our simulations, motivated by the fact that the mechanisms we identify are somewhat different from those previously discussed in the literature. In particular, we find that the growth of the *in situ* halo is very closely related to the accretion of satellites responsible for the growth of the canonical '*ex situ*' halo.

We proceed as follows. We describe our simulations in Section 2. In Section 3 we explain how we identify *in situ* halo stars and in Section 4 we examine their origins. Section 5 describes the present-day properties of our *in situ* halo. Section 6 investigates the satellite progenitor of *in situ* stars formed from stripped gas. In Section 7 we interpret our results, discuss the limitations of *in situ* halo models based on hydrodynamical simulations and compare with similar studies. A summary of our conclusions is given in Section 8. A detailed comparison with the results of T12 and T13 is included in Appendices A and B, along with a short discussion of numerical convergence.

Table 1. Numerical parameters adopted for the three simulations: DM and gas particle masses and the maximum gravitational softening length in physical units (defined as the scale of a Plummer kernel equivalent to the actual spline kernel used in the simulation).

	$M_{DM}(M_\odot)$	$M_{gas}(M_\odot)$	ϵ_{phys}[pc]
Aq-C	2.6×10^5	5.8×10^4	257
Aq-D	2.2×10^5	4.8×10^4	257
Aq-E	2.1×10^5	4.7×10^4	257

2 SIMULATIONS

We examine the stellar haloes that form in three smoothed particle hydrodynamics (SPH) simulations of Milky Way-mass galaxies. Dark-matter-only versions of these simulations formed part of the Aquarius project (Springel et al. 2008) and we retain the Aquarius nomenclature for our three sets of initial conditions, labelling them Aq-C, Aq-D and Aq-E. The DM resolution (particle mass) in our SPH simulations is similar to that of the 'level 4' simulation set in Aquarius.

The Aquarius DM haloes were themselves extracted from a cosmological simulation in a cube of comoving volume $100^3\,\mathrm{Mpc}^3$. They were chosen to have masses close to that of the Milky Way ($\sim 10^{12}\mathrm{M}_\odot$) and to avoid dense environments (no neighbour exceeding half the mass of the target halo within $1h^{-1}$Mpc; Navarro et al. 2010). Initial conditions for a resimulation of each halo were created with a 'zoom' technique, with higher mass boundary particles used to model the large scale potential and lower mass particles in an $\sim 5h^{-1}$Mpc region surrounding the target halo. Extra power was added to the initial particle distribution on small scales in the high resolution region, as described by Frenk et al. (1996). The numerical parameters for each simulation, including the particle masses and gravitational softening lengths, are listed in Table 1. We assume a ΛCDM cosmology, with parameters $\Omega_\mathrm{m} = 0.25$, $\Omega_\Lambda = 0.75$, $\Omega_\mathrm{b} = 0.045$, $\sigma_8 = 0.9$, $n_\mathrm{s} = 1$ and $H_0 = 100h\,\mathrm{km\,s^{-1}\,Mpc^{-1}} = 73\,\mathrm{km\,s^{-1}\,Mpc^{-1}}$.

Our simulation code is based on an early version of the PM-Tree-SPH code GADGET-3. Baryon processes are modelled as described in Okamoto et al. (2010) and Parry et al. (2012). Briefly, each gas particle represents an ISM with separate 'hot' and 'cold' (star-forming) phases. Gas particles above a critical density ($n_\mathrm{H} > 0.1\,\mathrm{cm}^{-3}$) are assigned a cold phase mass according to their thermal energy and a local pressure according to a polytropic equation of state. Gas in the cold phase is converted to stars at a rate inversely proportional to a local dynamical time, which in turn depends on analytic approximations for the effective pressure and distribution of cold cloud sizes. Our code follows the nucleosynthetic production of individual elements separately, in particular the iron yields of Types II and I SNe. Mass, metals and energy returned by evolved stars and their SNe are smoothly distributed over 40 near neighbour gas particles. The effective metallicity used to calculate the radiative cooling rate of a given particle is also a smoothed average. Kinetic energy is imparted directly to particles subject to SNe feedback, in proportion to the local velocity dispersion of DM. Particles are entrained in SN winds on a probabilistic basis and launched perpendicular to the plane of the

galactic disc. Wind particles are decoupled from the hydrodynamical calculation until they reach an ambient density $n_{\rm H} < 0.01\,{\rm cm}^{-3}$ or the time they have been decoupled exceeds a limiting time. Parry et al. (2012) improve the treatment of fluid instabilities in the hydrodynamic scheme of Okamoto et al. (2010) by incorporating artificial conductivity (Price 2008) and a time-step limiter (Saitoh & Makino 2009); they also adjust the treatment of SN winds to reduce the resolution dependence of mass loading and deposit thermal rather than kinetic energy from Type Ia SNe. The most relevant effect of these improvements is to suppress the formation of stars in cooling instabilities in diffuse circumgalactic gas (e.g. Kaufmann et al. 2006; Kereš et al. 2012; Hobbs et al. 2013). In the results we present below, we explicitly identify stars formed through such instabilities and find that they contribute $\lesssim 20$ per cent of the mass of the *in situ* stellar halo in our simulations. This fraction depends somewhat on resolution (becoming larger at lower resolution) as we discuss in Appendix B. Other modelling uncertainties are also discussed in Section 7 and Appendix B.

Details of two of our three hydrodynamical simulations (Aq-C and Aq-D) have been presented previously in studies that focused on satellite galaxies (Parry et al. 2012) and pseudo-bulge formation (Okamoto 2013). The luminosity function and luminosity–metallicity relation of the simulated satellites are comparable to those of dwarf galaxies in the Local Group. All three simulations result in galaxies with massive centrifugally supported discs as well as dispersion supported spheroids.

3 SAMPLE DEFINITION

The first step in defining our stellar halo sample is to identify all stars belonging to the central (Milky Way-analogue) galaxy at the present day (redshift $z = 0$). We choose stars that lie within a radius r_{200} which encloses a sphere of mean density 200 times the critical value for closure ($r_{200} = 227$ kpc for Aq-C and Aq-D, 202 kpc for Aq-E). From this sample, we isolate the halo by excluding stars that belong to satellite galaxies within r_{200} and stars that belong to the main galaxy disc or an inner spheroid ('bulge'), as follows.

Satellite DM haloes and their galaxies are isolated using a version of the SUBFIND algorithm (Springel et al. 2001) adapted by Dolag et al. (2009) to identify self-bound substructures, taking into account the internal energy of the gas when computing particle binding energies. All star particles bound to DM subhaloes at $z = 0$ are excluded from our halo star sample.

The central galactic disc is identified by finding stars on orbits that are approximately circular and that lie close to a plane normal to the net angular momentum vector of the whole stellar component. A coordinate system is chosen such that the net angular momentum vector of all stars within $0.2r_{200}$ points in the positive z-direction. The circularity of each star's orbit is then defined as

$$\mathcal{E}_{\rm E} = \frac{J_z}{J_{\rm circ}(E)}, \qquad (1)$$

where J_z is the z component of the star's specific angular momentum and $J_{\rm circ}(E)$ is the specific angular momentum of a star with the same binding energy on a circular orbit. All stars with $\mathcal{E}_{\rm E} > 0.8$ are identified with the central galactic disc and excluded from our halo star sample.

Table 2. Total mass in the (outer) disc, 'bulge' and stellar halo regions of the $(r, \mathcal{E}_{\rm E})$ plane according to our criteria. The final row gives the fraction of mass in the stellar halo region that is formed *in situ*. Our galaxies are roughly half the mass of the Milky Way; note that the disc mass quoted is only for stars with $r > 5$ kpc. Our 'bulge' definition includes all stars with $r < 5$ kpc, regardless of their kinematics (it does not correspond to a specific kinematic or photometric component in our simulations or in real galaxies).

		Aq-C	Aq-D	Aq-E
Mass ($10^9 {\rm M}_\odot$)	Disc ($r > 5$ kpc, $\mathcal{E}_{\rm E} > 0.8$)	3.0	4.3	4.3
	Bulge ($r < 5$ kpc)	34.5	21.9	25.2
	Halo ($r > 5$ kpc, $\mathcal{E}_{\rm E} < 0.8$)	4.6	8.4	6.8
In situ halo fraction		37%	33%	41%

Fig. 1 shows the distribution of stellar circularity as a function of radius in our three simulations. A concentration of corotating stars on near-circular orbits extending to ~ 30 kpc is obvious in all cases, which we identify with the thin disc. A number of streams on pro- and retrograde orbits are also visible at large radii.

At $r \lesssim 5$ kpc the density of stars on non-circular orbits is comparable to the density of stars in the disc. We identify this complex region with a galactic 'bulge' (using the term loosely, since this region is substantially more extended than the bulge of the Milky Way). To simplify our definition of the stellar halo, we exclude *all* stars with $r < 5$ kpc, regardless of circularity. This cut is easy to apply to both models and data. It also follows the loose convention of most Milky Way stellar halo work, in which stars more than a few kiloparsecs interior to the solar neighbourhood are excluded (the exception being those high above the disc plane) even though the inward extrapolation of a canonical r^{-3} density profile would predict a substantial mass of halo stars in the centre of the Galaxy (see also the discussion in Cooper et al. 2010).

Fig. 1 further separates star particles into accreted (middle row) and *in situ* (bottom row) according to whether or not they are bound to the main branch progenitor of each DM halo at the first snapshot after their formation. Star particles that are first bound to a DM halo other than the main progenitor are considered as accreted, even if they form in a subhalo of the main branch (i.e. if they form in a satellite galaxy of the Milky Way analogue) and are subsequently stripped[1]. Table 3 summarizes the total mass of the stellar halo and the relative proportion of *in situ* stars.

Fig. 2 shows the mean density of accreted and *in situ* halo stars in spherical shells centred on the galaxy. The profile of the *in situ* halo has a similar shape and amplitude in all three simulations, with a slight steepening evident in the 'bulge' region of Aq-C. In both Aq-C and Aq-D, the accreted halo stars are less centrally concentrated than the

[1] This is an important difference with the work of T13, who included stars formed in bound satellites within r_{200} in the *in situ* halo as part of their 'endo debris' category.

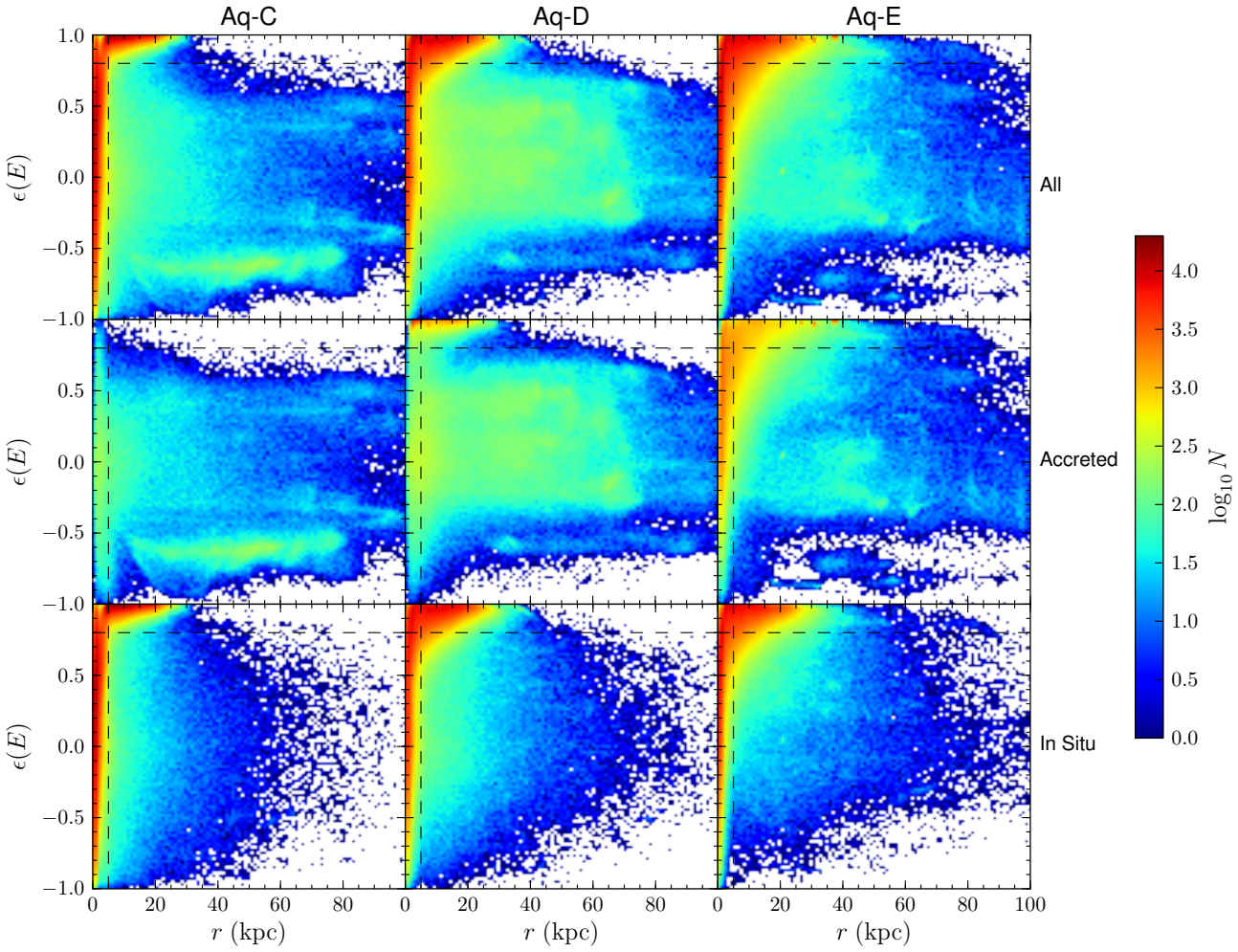

Figure 1. The distribution of stars in radius-circularity space for Aq-C (left column), Aq-D (centre column) and Aq-E (right column). Panels in the top row include all stars bound to the main DM halo ($r < 90$ kpc), while the middle and bottom rows include only accreted and *in situ* stars respectively. Dashed horizontal lines indicate the circularity cut used to define disc stars. Dashed vertical lines mark the 5 kpc cut in radius used to define 'bulge' stars. All stars outside these regions are classified as halo stars. The colour scale corresponds to the logarithm of the number of star particles.

in situ component, with a mild break due to accreted stars alone at $70 < r < 90$ kpc, while in Aq-E the two components are almost indistinguishable. The accreted–*in situ* transition in these profiles at ~ 20 kpc is consistent with the average for Milky Way analogues in the GIMIC simulation (Font et al. 2011).

Aq-D and Aq-E have 'thick' discs with a high degree of non-circular motion, apparent in the top row of Fig. 1 as a high density of stars at $0.5 < \mathcal{E}_{\rm E} < 0.8$ and $5 < r < 20$ kpc. According to the aforementioned cuts on circularity and radius, we classify these as halo stars. However, examining the variation of the circularity distribution with height above the disc plane reveals that these stars simply make up the low-circularity tail of a continuous distribution. The fraction of stars on circular orbits is highest close to the plane.

The most important question from the point of view of this paper is not the origin of thick disc stars, but whether or not they can, or should, be distinguished as a separate galactic component. Our simulations differ greatly in this respect, in line with earlier studies of the origin and structure of thick discs in simulations (e.g. Sales et al. 2009). Fig. 1 shows that accreted stars can make a significant contribution to the 'disc'. In Aq-D, they contribute mainly to the 'thin' disc – the thick disc is formed *in situ*. In Aq-E, accreted and *in situ* 'disc' stars contribute at a similar ratio over a wide range of circularity and radius.

In the context of observations of the Milky Way, a geometrically oblate stellar component, intermediate between disc and halo, was identified by Yoshii (1982) and Gilmore & Reid (1983), but optimal and objective ways to classify this component are still under debate (see, for example, recent reviews by Ivezić et al. 2012; Rix & Bovy 2013). Classifications have been suggested based on metallicity and kinematics that imply different distinctions between thick disc and halo stars (Ivezić et al. 2008; Bovy et al. 2012; Rix & Bovy 2013; Schlesinger et al. 2014; Ruchti et al. 2015). The chemodynamical distribution functions of our three galaxies are different from one another, and almost certainly differ-

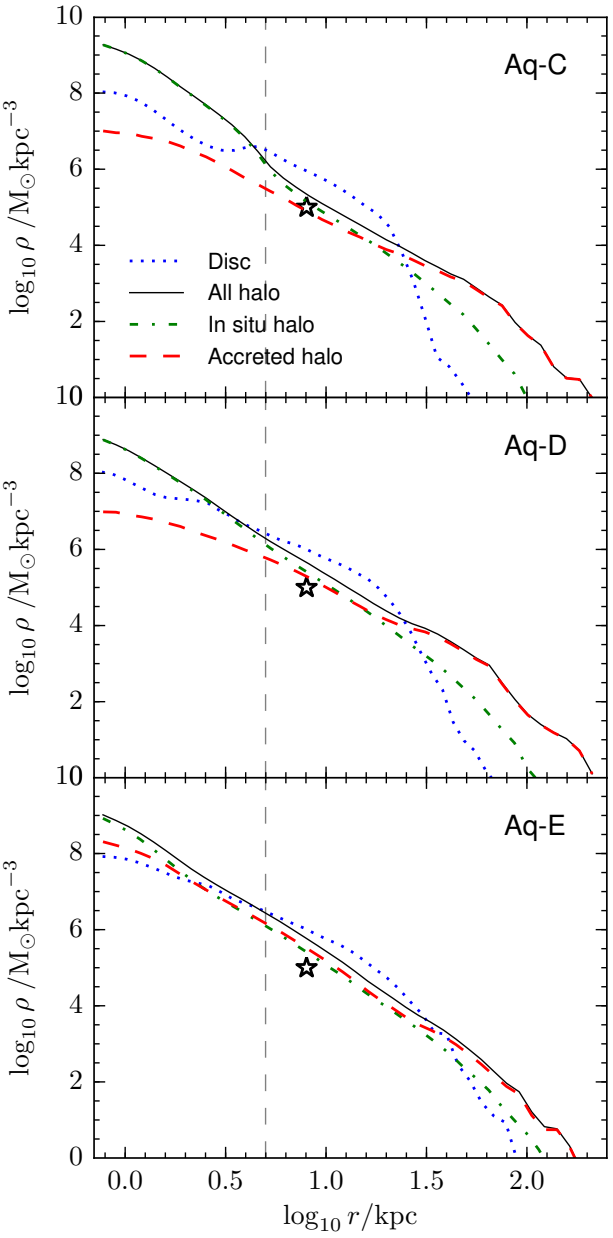

Figure 2. Spherically averaged stellar density profiles for Aq-C (top), Aq-D (centre) and Aq-E (bottom). The red dashed and green dot–dashed lines correspond to the accreted and *in situ* halo components respectively. The solid black line is the sum of these and can be compared to measurements for the Milky Way (black star; Fuchs & Jahreiß 1998; Gould et al. 1998). The blue dotted line corresponds to disc stars, selected by their orbital circularity. The minimum extent of the radial axis is set by the gravitational softening length for star particles. A grey dashed vertical line at 5 kpc marks the 'bulge' region that we exclude from our analysis of the stellar halo.

ent from the Milky Way distribution function on which these observational definitions are based. Therefore, we do not believe that additional cuts to separate a thick disc component from the thin disc and halo (for example, using a threshold metallicity, a limiting rotation velocity or vertical extent) are helpful for the interpretation of our simulations. This should be kept in mind when comparing our results to observations of the Milky Way.

Table 3. Breakdown of all *in situ* halo stars into three subtypes, according to their formation mechanism.

	Aq-C	Aq-D	Aq-E
Heated disc	2.8%	26.0%	31.0%
Stripped gas	59.8%	56.7%	56.9%
Smoothly accreted gas	37.3%	17.3%	12.1%

4 THE ORIGIN OF *IN SITU* STARS

In this section we look in more depth at the origin of the *in situ* component of the stellar halo. The density of this component exceeds that of accreted halo stars in the inner ~ 20 kpc of our galaxies. It may thus be very important for spectroscopic observations of halo stars in the solar neighbourhood and in surveys of main-sequence turnoff stars within a few kiloparsecs of the Milky Way disc plane.

In order to trace how *in situ* stars formed in our simulations, we separate them into three disjoint subcategories:

(i) 'heated disc' stars, which met the thin disc circularity criterion when they were formed, but are not in the disc at $z = 0$;
(ii) stars formed from 'stripped gas', brought into the main DM halo bound to a subhalo and subsequently stripped by tidal forces or ram pressure;
(iii) stars from 'smoothly accreted gas', which enters the main DM halo through direct (smooth) accretion.

Categories (ii) and (iii) are easily distinguished by tracing the DM halo membership history of the parent gas particle for each star particle. The gas from which heated disc stars form must originally have either been stripped from a subhalo or smoothly accreted, so these stars could also be classified into the second or third categories. However, in this case it is the fact that they formed in the thin disc and were scattered out of it, rather than how their parent gas particle arrived in the disc, that we consider to be most important.

The fraction of *in situ* halo stars in each category is shown in Table 3. It is clear that there is a large variation between the three simulations, although the *in situ* stars forming from gas stripped from satellites dominate in all cases. In the next section we discuss each category in more detail and compare their properties.

4.1 Heated disc stars

The central galaxies in our three simulations undergo several episodes of disc destruction and regrowth at $z > 3$. Over the redshift range $3 > z > 2$, a stable disc is established. This disc continues to grow until $z = 0$, although its angular momentum axis may precess. Our heated disc category only includes stars that once belonged to this stable disc. Stars on highly circular orbits may be scattered to more eccentric orbits by secular evolution and satellite impacts (e.g. Purcell et al. 2010). We refer to this loosely as 'heating', in the

Table 4. Properties of the present-day thin stellar discs in our three simulations, defined by circularity $\mathcal{E}_{\rm E} > 0.8$. Columns from left to right give formation redshift, mass fraction in place at formation redshift, and redshift at which half the $z = 0$ mass is in place.

	$z_{\rm form}$	$f_{\rm form}$	$z_{1/2}$
Aq-C	2.54	12%	0.92
Aq-D	2.32	8%	0.83
Aq-E	2.20	16%	0.76

sense of an increase in non-circular motion. These perturbed disc stars are likely to have a clear kinematic and chemical relationship to those in the present-day thin disc.

We identify all star particles in the $z = 0$ disc, as defined in Section 3, that exist in a given earlier snapshot and use these to define J_z (assuming that the number of star particles scattered *into* the disc is negligible). We then apply the circularity threshold $\mathcal{E}_{\rm E} > 0.8$ to identify all newly formed star particles in the disc at that snapshot. Any of these that have $\mathcal{E}_{\rm E} < 0.8$ at $z = 0$ are assigned to our heated disc category.

Beyond a certain redshift, $z_{\rm form}$, we can no longer reliably identify a stable progenitor of the $z = 0$ disc, and hence we cannot define J_z. This limit is due to the small number (< 100) of ancient disc stars and increasing frequency of fluctuations in the central potential that destabilize protodiscs. Table 4 gives $z_{\rm form}$ for each of our simulations, along with $z_{1/2}$, the redshift by which the $z = 0$ disc has assembled half its final mass. Table 4 also gives $f_{\rm form}$, the mass fraction of $z = 0$ disc stars that form earlier than $z_{\rm form}$. This fraction is no more than 16 per cent (Aq-E). Stars scattered from this unidentified protodisc (and any others discs that were completely destroyed before $z_{\rm form}$) are considered to fall into one of the other two *in situ* categories, according to the origin of their parent gas particle.

4.2 Stars from stripped gas and smoothly accreted gas

Halo stars can form directly in the circumgalactic medium, either in quasi-free-falling cold gas clouds (not associated with DM clumps) or the gaseous tidal or ram pressure stripped streams of satellite galaxies. We distinguish between these two possibilities based on whether or not the parent gas particle of a given star particle was bound to another DM halo before being bound to the main halo. Stars forming from stripped satellite gas particles may be chemically and kinematically similar to stars in the accreted stellar halo. In contrast, stars forming in gas condensing out of the hot hydrostatic gas halo, or other 'smoothly' accreted cold clumps, may have properties more similar to those expected of an *in situ* halo formed by monolithic collapse.

Fig. 3 shows the absolute star formation rate of each *in situ* category as a function of time elapsed since the big bang. These star formation rates are low compared to those typical of the stable disc and the progenitors of accreted stars ($\sim 1\,{\rm M}_\odot\,{\rm yr}^{-1}$). The majority of halo stars that form in stripped or smoothly accreted gas are more than 9 Gyr old, only marginally younger than the typical age of accreted

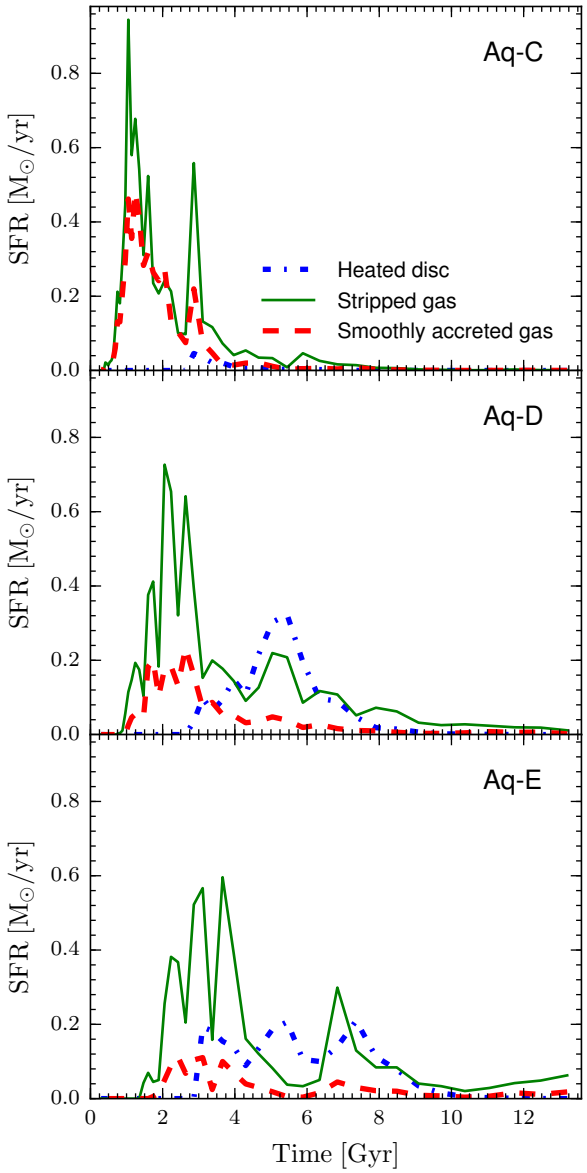

Figure 3. Formation history for *in situ* halo stars assigned to each of our three *in situ* formation mechanisms. Time is measured from the origin of the universe. Peaks in the formation of stars in smoothly accreted gas are clearly correlated with those in stripped gas at $t < 4$ Gyr. Vertical dotted lines mark $z_{\rm form}$ and $z_{1/2}$ as given in Table 4.

stars. In Aq-D and Aq-E, there are also ~ 2 Gyr-long bursts of *in situ* star formation starting at $t \approx 4$ and 6 Gyr respectively. Interestingly, these also correspond to episodes of formation for scattered disc stars (blue) and thin disc stars (not shown). These episodes correspond to the rapid infall of cold gas on to the disc during periods in which several relatively massive satellites are being disrupted simultaneously.

Another notable feature of Fig. 3 is that the star formation rate in smoothly accreted gas (red) is clearly correlated with that in stripped gas (green), especially in the dominant early epoch of *in situ* halo formation (ages > 9 Gyr). This correlation persists even if we select only stars forming at $r > 30$ kpc, far away from the disc, suggesting that the

conditions under which *most in situ* halo stars form are in fact related to the accretion and stripping of gas-rich satellites. It appears that star formation may be triggered by the mixing of free-floating gas from the hydrostatic halo with star-forming stripped gas. We also see corresponding peaks in the accreted halo star formation rate, suggesting that star formation is triggered in the infalling satellites as well.

These effects must arise from the subgrid model of star formation. They may therefore occur, to a greater or lesser extent, with other similar star formation prescriptions used in the literature. Since there are no unambiguous observational tests of the predictions of models for star formation in the diffuse circumgalactic gas, it is very difficult to judge whether or not the behaviour of a particular simulation is physically plausible (see also the discussion in Appendix B). Isolating dependencies on modelling uncertainties such as these is one of our motivations for separating simulated halo stars into categories based on their physical origin.

Regardless of how they actually form, the *classification* of gas particles as 'smoothly' accreted is resolution dependent: gas bound to a low-mass infalling DM halo, and so classified as 'stripped' at high resolution, would be classified as 'smoothly accreted' in a lower resolution simulation that does not resolve the parent halo. In Appendix B we conclude that, in our simulations, the uncertainty in the total mass of the smoothly accreted halo component is dominated by this classification uncertainty, rather than the resolution dependence of star formation efficiency.

5 IN SITU HALOES AT $z = 0$

In this section, we examine the observable characteristics of *in situ* halo stars at the present day, starting with a summary of halo properties and then looking in more detail at regions analogous to the solar neighbourhood.

5.1 Whole halo

Fig. 4 compares the spherically averaged density profiles of our three *in situ* halo categories and accreted halo stars. In the $r < 20$ kpc region where *in situ* halo stars dominate over accreted stars, they contribute roughly equal mass fractions; the exact proportions vary from halo to halo. We see a strong correspondence between stars formed from stripped and smoothly accreted gas at all radii, which, in combination with Fig. 3, suggests that they form with a similar distribution in both space and time. As expected, heated disc stars have a steeper profile, with most concentrated at $r < 20$ kpc.

Fig. 5 shows Toomre diagrams (Sandage & Fouts 1987) that compare the amplitude of circular and radial motion for different components. A galactocentric UVW velocity frame (e.g. Binney & Merrifield 1998, p. 627) is defined with respect to the thin disc in each simulation.

Of the three simulations, the stellar halo in Aq-C has kinematic properties most similar to those measured for the Milky Way. The peak rotational velocity of the disc is $\sim 220\,\mathrm{km\,s^{-1}}$. The heated disc stars (blue) rotate in the same sense as those on circular orbits, with a lag of ~ 40–$180\,\mathrm{km\,s^{-1}}$. Stars formed from stripped and smoothly accreted gas are kinematically indistinguishable from each other, once again pointing to a close correlation between the

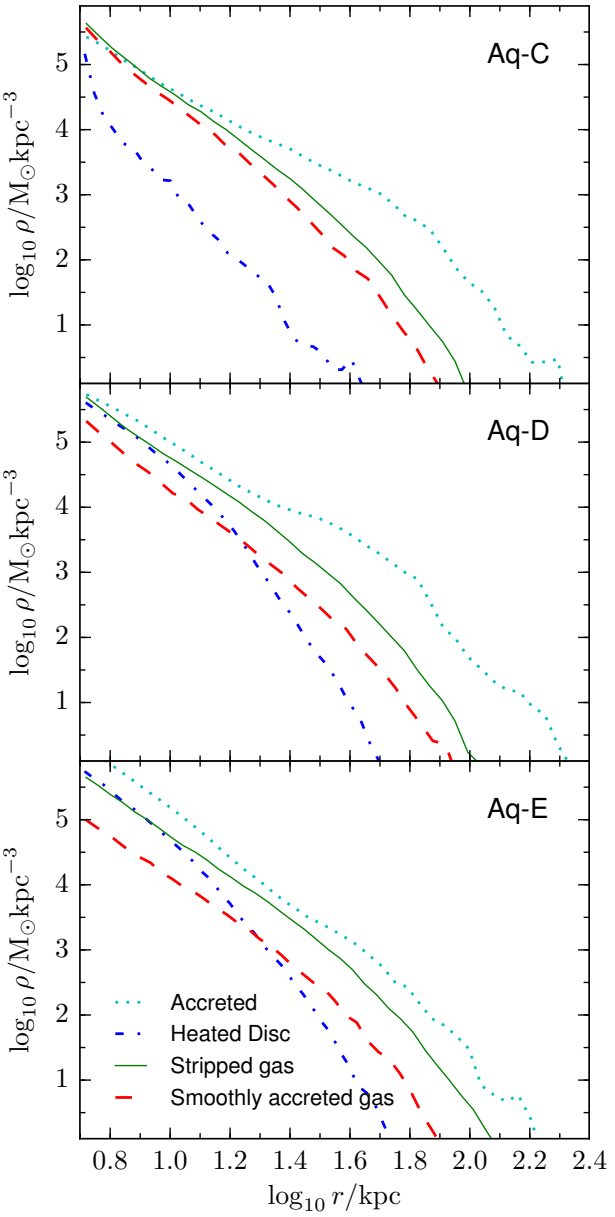

Figure 4. Spherically averaged density profiles of halo stars in the accreted and three *in situ* components for Aq-C (top), Aq-D (centre) and Aq-E (bottom).

dynamics of the two components. In the Toomre diagram they resemble the classical Milky Way halo, with zero net rotation and high radial velocity dispersion. Accreted halo stars show a similar distribution overall, but with notable overdensities due to individual streams, some of which have a net retrograde motion.

The heated disc stars in Aq-D and Aq-E have similar kinematics to those in Aq-C, but the stripped/smooth *in situ* haloes have a greater net rotation. In Aq-E, all three components once again resemble one another, although the stripped- and smooth-gas halo stars have a greater velocity dispersion. An underlying stripped/smooth *in situ* halo may still be present, but the bulk of *in situ* halo stars are more similar kinematically to the Milky Way thick disc. The be-

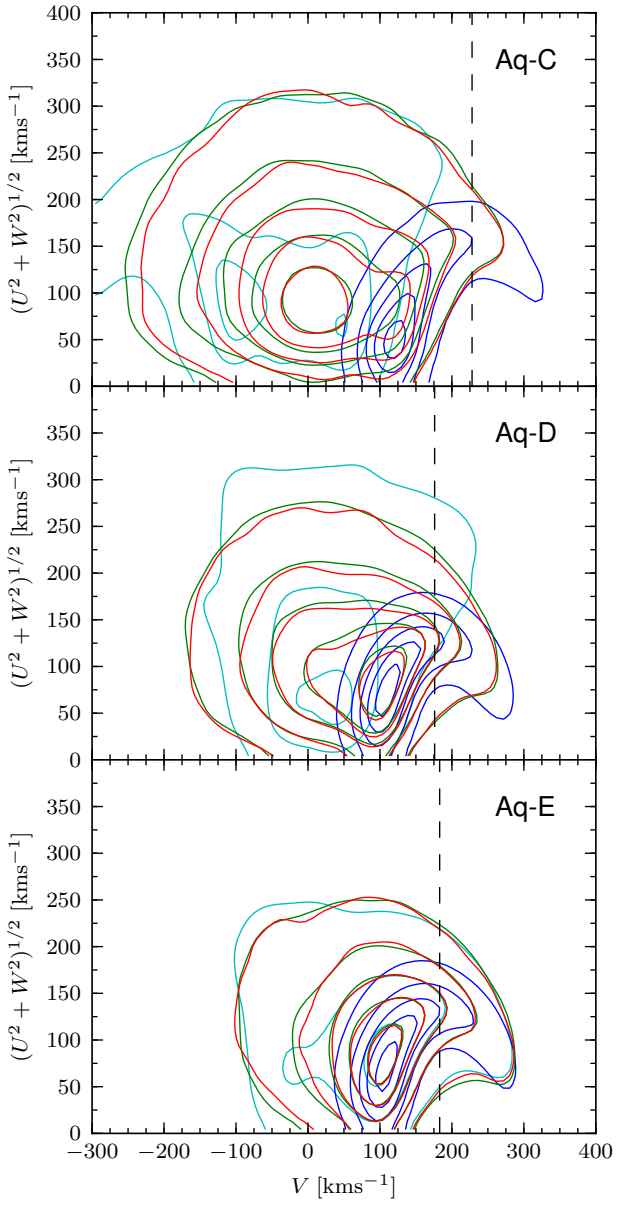

Figure 5. Toomre diagrams of the whole stellar halo. For stripped-gas, smooth-gas and heated disc *in situ* halo stars (red, green and dark blue respectively), contours mark the regions enclosing 10, 30, 50, 70 and 90 per cent of the stellar mass. For the accreted halo (cyan) only 10, 50 and 90 per cent levels are shown. The dashed vertical line marks the rotation velocity of the disc at 8 kpc.

haviour of accreted stars once again resembles that of the *in situ* component, even to the extent that they have a strong prograde rotation in Aq-E. Accreted halo components with prograde rotation were noted by Abadi et al. (2003) and also found in Milky Way-like systems in the GIMIC simulations (Font et al. 2011; McCarthy et al. 2012)

Finally, in Fig. 6, we examine the normalized metallicity distribution functions (MDFs) of each component of the *in situ* halo. Heated disc stars have the highest median [Fe/H] and narrowest dispersion. Their MDF resembles that of the thin disc, but is slightly more metal poor (by ~ 0.5 dex in Aq-C). Both *in situ* and accreted halo stars are systematically more metal poor than heated disc stars.

The MDF of *in situ* halo stars formed from stripped gas is very similar to that of accreted satellite stars, with a median systematically higher by no more than 0.1 dex. This is to be expected, as the dense cold gas stripped from satellites will have been enriched by the same stellar populations that make up the accreted halo. Moreover, very similar distributions will also result if prolonged star formation occurs in satellite galaxies while their gas is being stripped. The overall *in situ* MDF is close to that of the stripped-gas stars, since they dominate the *in situ* mass budget.

Looking in detail, the degree of similarity between the MDFs of the various components varies in each of our three simulations. This may depend on the extent to which the satellite galaxies contributing the bulk of stripped-gas stars are the same as those that contribute the majority of accreted stars. Since gas can be more easily expelled from shallower potentials, the most massive and metal-rich accreted progenitor galaxies are likely to retain the most gas when they enter the main DM halo. Stars stripped from these galaxies are expected to dominate the accreted halo, particularly near the centre. We investigate the relative contributions of star-forming stripped gas and directly accreted stars from different progenitors in Section 6 below.

Of the different *in situ* components, it is the stars that formed from smoothly accreted gas that have the lowest median metallicity and the broadest dispersion. This is consistent with the expectation that the gas surrounding each galaxy will be a mix of its own metal-rich ejecta and a large quantity of 'pristine', or only marginally enriched, gas from direct cosmological infall (Crain et al. 2010). In our simulations, the MDF is the only clear distinction between 'smooth gas' stars and 'stripped gas' halo stars.

5.2 The Solar Neighbourhood

As a rough analogue of the solar neighbourhood region most relevant to current observations, we examine the average properties of halo stars in a torus of cross-sectional diameter 4 kpc and galactocentric radius $r = 8$ kpc in the plane of the thin disc.

Table 5 summarizes the fraction of stars in each component. For a more direct comparison to the real data, we have grouped heated disc stars and stars that meet our thin disc circularity cut into a single disc component, because the typically high circular velocities of heated disc stars would most likely result in them being classified as 'thick disc' rather than halo stars in observations. Approximately 10 per cent of the stellar mass then remains in a component resembling the 'classic' halo, of which accreted stars contribute between 34 and 67 per cent.

Toomre diagrams in this region are almost identical to those in Fig. 5. The biggest differences in comparison to the overall halo are found in the solar neighbourhood MDFs, which are shown in Fig. 7. Stars formed from smoothly accreted gas that end up in the solar neighbourhood are more metal rich on average, such that their MDF has a very similar shape and amplitude to the accreted halo. This may be because the metal-poor contribution of this component seen in Fig. 6 is dominated by stars forming at large radii from gas that has not been polluted by the galactic wind of the

Table 5. Breakdown of all stars in the solar neighbourhood. Heated disc stars are grouped together with thin disc stars in this table. The top two rows give fractions of total stellar mass, while the lower three rows give fractions of stellar halo mass (second row) only.

Mass (10^8 $M_\odot$)	Aq-C	Aq-D	Aq-E
Disc stars (thin + thick)	26.4 (92.3%)	27.4 (88.7%)	28.0 (83.0%)
Halo stars	2.21 (7.7%)	3.49 (11.3%)	5.72 (17.0%)
Accreted	0.747 (33.9%)	1.79 (51.1%)	3.83 (67.0%)
Stripped gas	0.837 (37.9%)	1.23 (35.3%)	1.53 (26.7%)
Smoothly accreted gas	0.618 (28.0%)	0.476 (13.6%)	0.356 (6.23%)

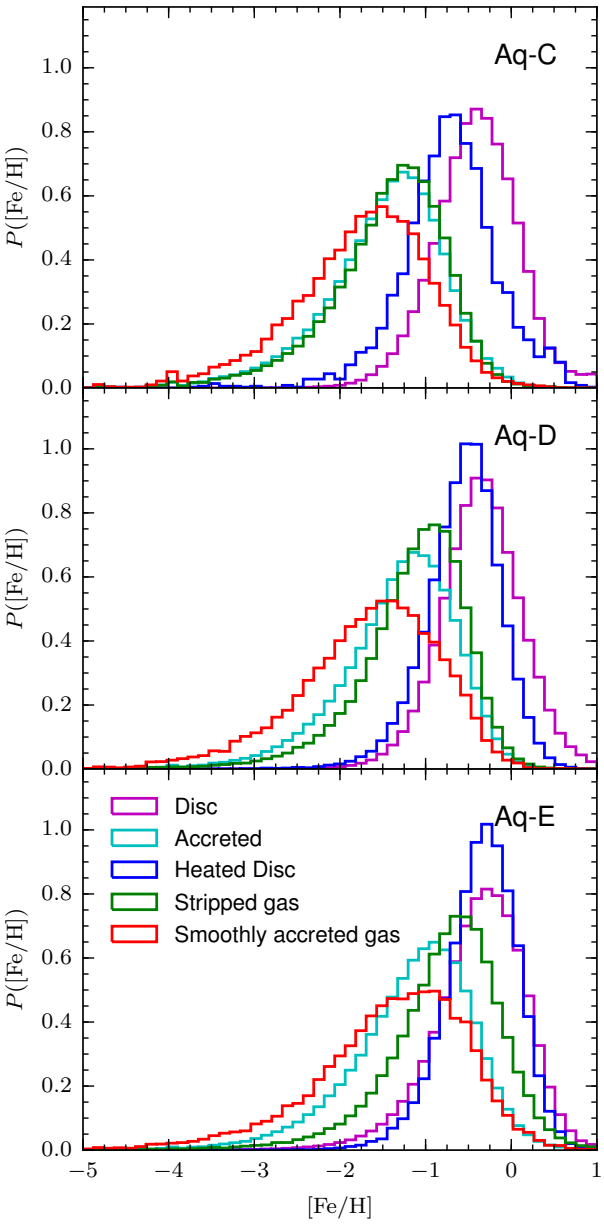

Figure 6. [Fe/H] distributions for the disc, accreted halo and three *in situ* halo components. Distributions are normalized by the total mass of stars in each component.

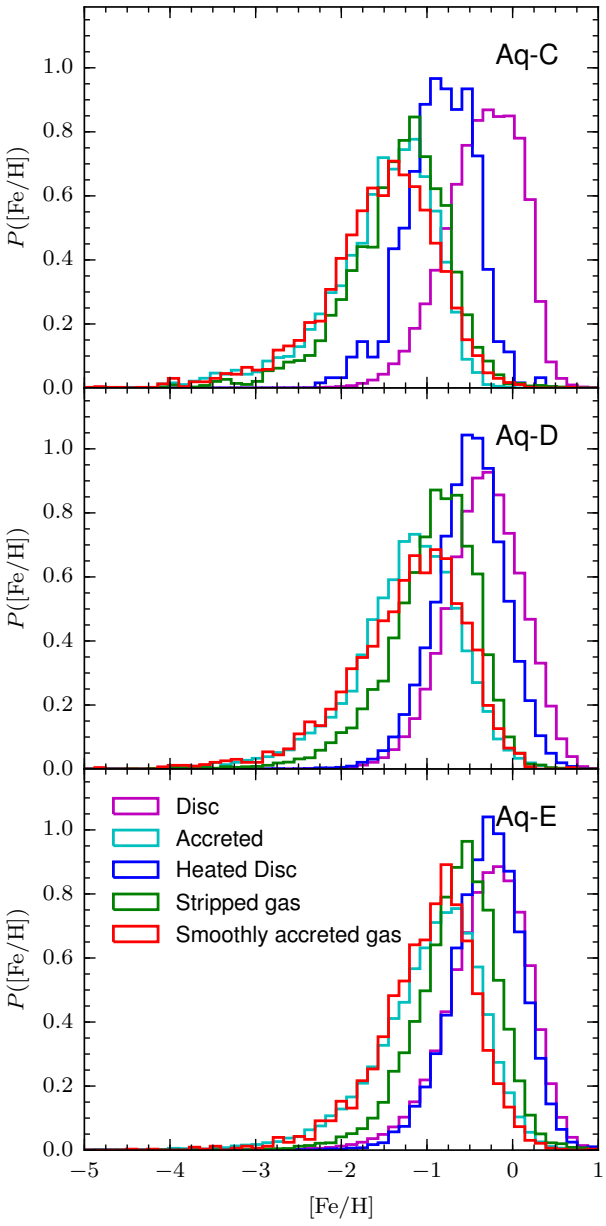

Figure 7. MDFs, as Fig. 6, but here in the solar neighbourhood.

central galaxy. Other components have the same relationship to one another as those in Fig. 6. Hence, we find no substantial differences between the properties of the *in situ* halo in the solar neighbourhood and the *in situ* halo overall. This is not surprising because we have already seen that the bulk of the *in situ* halo is concentrated within $r \lesssim 20$ kpc.

6 SATELLITE PROGENITORS

We have shown that our simulated stellar haloes are dominated by satellite accretion: the bulk of halo stars are stripped directly from satellites, and the majority of '*in situ*' halo stars form from gas stripped from satellites. However, as Fig. 2 demonstrates, stars formed *in situ* from stripped gas have a more centrally concentrated spatial distribution at $z = 0$ than directly accreted stars. In this section we examine the satellites which contribute to the halo, with the aim of determining how their infall times, masses and baryonic content affect the spatial distribution of the *in situ* and accreted components.

We first ask whether the subset of satellite progenitors contributing the gas from which an *in situ* stellar halo forms is the same subset contributing accreted stars. Fig. 8 compares the mass fractions of stars formed from stripped gas and directly accreted stars associated with each progenitor satellite. In all three simulations, satellites that contribute significantly to one component also tend to contribute significantly to the other. There is substantial variation in detail between the three haloes, reflecting their different accretion histories. A larger scatter is apparent in Aq-D, as well as a noticeable fraction of gas-poor contributors (lower-right area of the plot) relative to Aq-C and Aq-E. A larger fraction of those satellites also survive to $z = 0$ without being disrupted (blue points). The smaller number of surviving satellites in Aq-C reflects a quieter recent merger history.

In Fig. 9 we isolate the top three satellite progenitors of the stripped-gas *in situ* component and plot the density profiles of the accreted and stripped-gas stars they contribute. Aq-E stands out as having the most similar profiles for the two components, both of which are slightly steeper than the total accreted profile. In this case, the satellites plotted account for around 40 per cent of the total stripped-gas halo. With the possible exception of accreted stars in Aq-C, both accreted and stripped-gas stars from the top three satellites are distributed like the bulk of the stellar halo.

Fig. 9 suggests that the greater central concentration of the stripped-gas halo profile is not simply because most of the progenitor gas particles originate in more massive progenitors, which sink more rapidly through the action of dynamical friction. If that were the case, we might also expect stars accreted from the same progenitors to be more centrally concentrated than the accreted halo overall. Instead, we see that the debris profiles of the three most massive individual progenitors are very similar to the profile of the entire accreted halo. In our simulations, at the present day, accreted stars are distributed (on average) over the same range of radii at which they were liberated from their parent satellites. Conversely, we have confirmed that the stripped-gas particles from which *in situ* halo stars form dissipate some of their orbital energy between the times of stripping and star formation. The present-day distribution of the stripped gas halo is therefore imprinted at the time those stars form, rather than the time at which their parent gas particles are stripped.

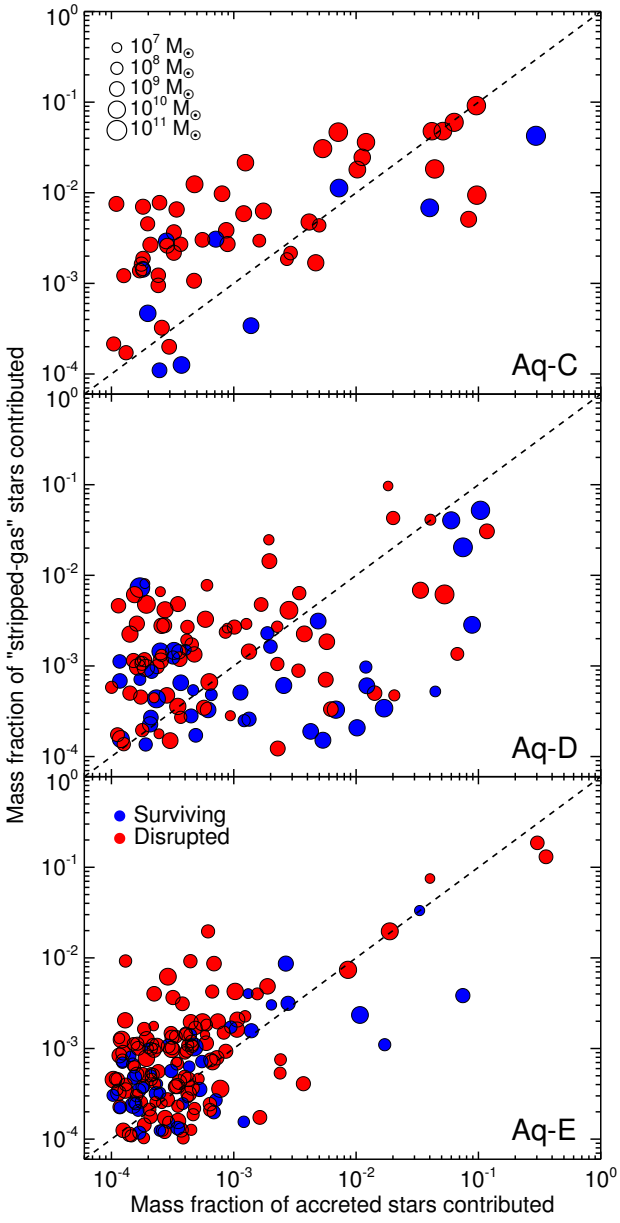

Figure 8. Mass fraction of the accreted halo and stripped-gas halo contributed by disrupted (red) and surviving (blue) satellite galaxies. The sizes of the points are proportional to the logarithm of the satellite's total mass at infall, as shown by the legend in the first panel. The diagonal dashed line indicates an equal fractional contribution to the accreted and stripped-gas components.

7 DISCUSSION

Our finding of accretion-triggered star formation in smoothly accreted gas may be, at least in part, a consequence of our hydrodynamics scheme. In some hydrodynamic models, cold clouds can condense independently of

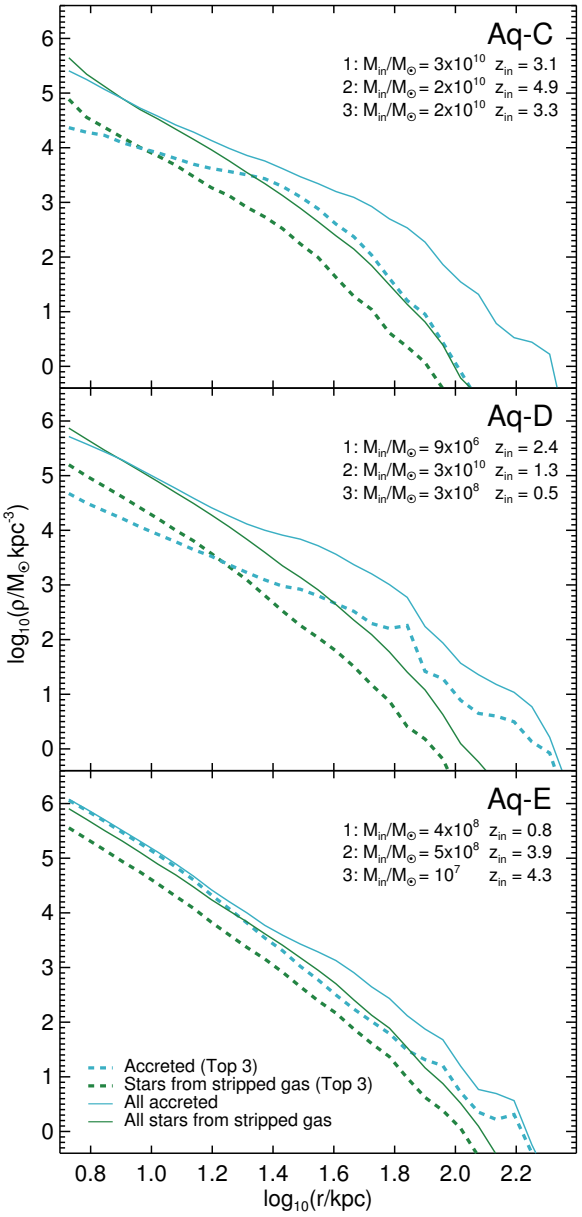

Figure 9. Spherically averaged density profiles of halo stars associated with the top three contributors to the 'stripped-gas' component. The profiles of stars formed from gas contributed by those galaxies are shown as dashed, cyan lines, while the profile of stars accreted from those satellites directly are shown as solid, green lines. Thinner, black lines of the same styles show the corresponding total profiles.

tidally stripped gas, while in others, condensation and mixing by fluid instabilities may both be suppressed (e.g. Kaufmann et al. 2006; Kereš et al. 2012; Parry et al. 2012; Hobbs et al. 2013). As we noted in Section 4.2, there are no strong observational test of different models at this level of detail. In Appendix B, we carry out a simple resolution study of the smoothly accreted gas component. At lower resolution, more baryons are retained by the main halo and relatively more of these baryons are classified as smoothly accreted. The overall efficiency with which smoothly accreted gas is converted to stars also varies systematically with resolution, although (in our simulations) this is a minor contribution to the change of *in situ* stellar halo mass, relative to the first two effects.

Given such uncertainties, it is worth noting that, with a single SPH code, the different cosmological initial conditions of our three simulations result in markedly different *in situ* halo properties at $z = 0$. It is obvious that the mass spectrum, arrival time distribution and prior star formation histories of accreted satellites directly determine the properties of the accreted halo. Remarkably, however, in our SPH simulations, these factors are also extremely important in the formation of the *in situ* halo. Without satellite accretion, there would be hardly any *in situ* halo stars in our simulations. Moreover, it is unlikely that all the stars we classify as heated disc halo stars would be considered as such by observers. The vast majority are on orbits of moderate circular velocity, corotating and coplanar with the thin disc, and would likely be classified as 'thick disc' stars as discussed in Section 3. In Aq-C, a large fraction of these stars belong to the end of a bar in the galactic plane that extends slightly beyond our 'bulge' cut at 5 kpc.

Our model is clearly not unique. Nonetheless, our *in situ* haloes are compatible with the basic observable properties of the Milky Way's stellar halo, if we exclude scattered disc stars. Stars formed from stripped and smoothly accreted gas in the main halo are old and metal poor, with a significant tail to low metallicity. The kinematic and chemical similarities are closest in Aq-C, which also has the most Milky Way-like thin disc.

Two of our haloes conform to the expectation from earlier work that *in situ* halo stars are more concentrated than accreted stars, but in the third, the *in situ* and accreted halo density profiles are almost identical. Interestingly, it is only in this third case that there is a significant difference in the MDFs of *in situ* and accreted stars.

McCarthy et al. (2012) studied the origin of *in situ* halo stars in 412 Milky Way-mass galaxies from the GIMIC simulations, which have a DM particle mass ~ 300 times larger than our simulations. With the same definition of disc stars and accreted stars, they find *in situ* halo mass fractions ranging from 20 to 60 per cent. Their *in situ* stars are, on average, younger and more metal rich than their accreted halo stars, with a centrally concentrated oblate distribution and prograde rotation. They demonstrate that these properties result from star formation at $z \sim 1$ in 'proto-discs' that are subsequently destroyed.

Although our three simulations produce total *in situ* mass fractions consistent with the distribution found by McCarthy et al. (2012), there are some notable differences in the origin of *in situ* stars. Accreted gas is the dominant contributor to our *in situ* haloes, whereas McCarthy et al. find that approximately half of their *in situ* halo mass is formed from gas that is shock-heated to the virial temperature of the main DM halo. Our *in situ* DM haloes form at somewhat higher redshift and we can trace back our $z = 0$ discs to $z \sim 2.5$, supporting the suggestion of McCarthy et al. that the Aquarius simulations have quieter-than-average accretion histories. As McCarthy et al. do not compute the fraction of gas forming their *in situ* component that was previously bound to satellites, it is likely that their proto-

disc stars mix together both stripped and smoothly accreted gas, and possibly some fraction of our heated disc population. Font et al. (2011) note that formation from stripped gas is apparent in the same set of galaxies from the GIMIC simulations and is likely responsible for their *in situ* stars at $r > 20$ kpc. We find that this mode of formation dominates at somewhat smaller radii. This may be a consequence of the better spatial resolution in our simulations; a smaller gravitational softening length means satellite gas tends to be more tightly bound, allowing it to sink further into the potential before being stripped by ram pressure or tidal forces (see also Parry et al. 2012).

As noted in the introduction, a series of papers by Tissera et al. (T12, T13, T14) examine *in situ* halo stars in six SPH simulations from the Aquila suite (Scannapieco et al. 2012). They also use GADGET-3 for these simulations, but with different implementations of subgrid physics and slightly lower resolution (a factor of 5 in DM particle mass; Scannapieco et al. 2012). Two of their simulations, Aq-C and Aq-D, have the same initial conditions as the simulations with the corresponding labels in this paper. To aid the reader in comparing our results with this series of papers, we comment here on the differences between our sample definitions and those of Tissera et al.

T12 separated disc and halo stars with a circularity cut, $J_z/J_{\rm circ}(E) > 0.65$, which classifies many more stars as 'disc' than our cut. Also, they did not restrict the height of disc stars above the mid-plane. They excluded bulge stars with an energy criterion that roughly equates to a radius of 5 kpc, comparable to our 'bulge' cut (see T12).

In the analysis of Tissera et al., *in situ* halo stars are divided into 'inner' (more bound) and 'outer' (less bound) populations according to a cut in relative binding energy. This equates to a radial cut in the range $14 < r < 36$ kpc (15 and 19 kpc for Aq-C and Aq-D respectively). They further subdivided these populations by origin, according to whether the stars were formed outside the virial radius ('debris') or inside ('endo-debris'). This definition is different from ours, which counts a present-day halo star particle as 'accreted' if it formed bound to a satellite subhalo, regardless of whether the satellite was inside or outside the virial radius of the main DM halo at the time. This may not be significant, because the fraction of accreted halo stars formed in bound satellites after their infall is typically small (see McCarthy et al. 2012).

The definition of heated disc halo stars in T13 requires the star particle to have $J_z/J_{\rm circ}(E) > 0.65$ at its formation. Our definition also requires those stars to have been scattered from the disc that survives at $z = 0$; we would classify some fraction of their heated disc stars as formed from either stripped or smoothly accreted gas. This may explain why T13 find a much larger heated disc fraction in Aq-C despite their less stringent disc circularity cut (indeed, they note that heated disc stars have retrograde rotation in one of their simulations).

Allowing for these differences of definition between our study and that of T13, a number of similarities are clear. The dominance of *in situ* over accreted halo stars in our simulations at $r \lesssim 20$ kpc is also seen in their 'inner halo' populations. Moreover, they also find that scattered disc stars make a negligible contribution outside this region. The kinematic properties, as shown in our Fig. 5, are similar. In Aq-C and Aq-D, T13 report a median [Fe/H] of endo-debris stars lower than those of debris stars by 0.17 and 0.26 dex, respectively. This is the opposite of what we find, but could be easily explained if the T13 endo-debris definition includes a similar or larger fraction of stars formed from smoothly accreted gas. This is supported, at least qualitatively, by our findings in Appendix A, which indicate first that the star formation efficiency for the central galaxy is much higher in the Tissera et al. simulations, and secondly that stars in our simulations meeting the Tissera et al. endo-debris definition are predominantly formed in satellites *after* their accretion by the main halo.

Recently, Pillepich et al. (2015) described the *in situ* stellar halo of the *Eris* simulation (a zoom of an isolated halo, $M_{200} = 8 \times 10^{11} {\rm M}_\odot$, forming a late-type galaxy with $M_\star = 3.9 \times 10^{10} {\rm M}_\odot$; Guedes et al. 2011). The particle mass of *Eris* is $\sim 1/3$ of that in our simulations. They find a transition in the density profile between *in situ* stars (including the disc) and accreted stars at ~ 10 kpc. Having cut out a cylinder of height ± 5 kpc and radius 15 kpc to excise the disc and bulge, they define an inner halo (all stars $r < 20$ kpc excluding this cylinder) and an outer halo (all stars $20 < r < 235$ kpc). They find that ~ 25 per cent of stars in their inner halo were formed *in situ*, falling to only 3 per cent in their outer halo. Applying the same cuts to our haloes C, D and E, we find *in situ* fractions of $(83, 78, 76)$ per cent for an equivalent inner halo region and $(29, 31, 65)$ per cent for an equivalent outer halo region. These much larger fractions are most likely because Pillepich et al. count both disc and halo stars in their definition of *in situ* stellar mass – our discs are larger than the disc of *Eris* and hence are not excised completely by their geometric cut. If we count only our halo stars in these regions (excluding disc stars by their circularity as above), the *in situ* mass fractions for our three simulations are $(20, 18, 15)$ percent in the Pillepich et al. inner halo and $(14, 11, 17)$ per cent in the outer halo. Larger 'outer halo' *in situ* mass fractions in our simulations may well result from differences between our subgrid models and those used for *Eris*, in particular their higher density threshold for star formation and neglect of metal line cooling in gas with temperature $> 10^4$ K (Guedes et al. 2011).

8 CONCLUSIONS

We find the following properties of *in situ* stellar halo stars in three high resolution SPH simulations of Milky Way analogues:

(i) The *in situ* stellar halo accounts for 30-40 per cent of the stellar mass outside the thin disc ($\mathcal{E}_{\rm E} > 0.8$) and inner spheroid ('bulge'; $r > 5$ kpc). This fraction includes stars that observers may classify as belonging to a thick disc.

(ii) The *in situ* halo dominates over the accreted stellar halo at $r < 30$ kpc in two out of our three simulations. In the third simulation, both *in situ* and accreted halo stars have almost the same volume density distribution.

(iii) Between 2 and 30 per cent of the *in situ* halo comprises stars scattered from near-circular orbits in the plane of the thin disc to more eccentric orbits. These form at lookback times of 5 to 9 Gyr, retain high circular velocities and have relatively narrow MDFs with median $-1 <$ [Fe/H] < -0.5. This component resembles the Milky Way's

thick disc, although we note that, in two out of our three simulations, kinematically selected eccentric/thick discs also have a significant contribution from both accreted stars and stars formed from accreted gas.

(iv) The rest of the *in situ* halo stars form in gas clouds in the circumgalactic halo, on highly eccentric orbits near the disc plane, or in the chaotic gas-rich stage of the galaxy's formation ($z > 2.5$), before a stable disc is established. In one simulation, these halo stars strongly resemble the 'classical' isotropic, metal-poor, dispersion-supported stellar halo of the Milky Way. In the other two simulations, most such halo stars have significant rotation in the same sense as the thin disc.

(v) We identify two distinct origins for these stars: gas that has been stripped out of satellite galaxies by tides and ram pressure, and gas that is incorporated directly into the 'smooth' halo of the main galaxy by cosmological infall and SN-driven outflow from the central galaxy.

(vi) Stars formed *in situ* from stripped gas have a very similar MDF to the accreted stellar halo, because this gas is brought in by the same progenitor satellites. Halo stars formed from smoothly accreted gas have a broader MDF and are, on average, the most metal poor of the components we identify.

(vii) The density profile of halo stars formed *in situ* from stripped gas is more concentrated than that of the stars accreted from the same progenitor galaxies. This reflects dissipative collapse of this stripped gas after it is liberated, rather than differences in how and when star and gas particles are stripped, or in the contributions of different satellites.

(viii) In all cases, among the *in situ* halo stars not scattered from the disc, there is almost no difference in the present-day phase-space distribution of those formed in stripped and smoothly accreted gas. The correspondence is so close that we suggest that, in our simulations, star formation in the hot gaseous halo is directly triggered by the passage of dense clumps of star-forming stripped gas.

(ix) The properties of *in situ* stars in the solar neighbourhood are representative of the *in situ* halo overall, except that stars formed from smoothly accreted gas in this region are notably more metal rich.

Based on these findings, we conclude that essentially *all* halo stars in our simulation are the result of cosmological accretion and merging, with no obvious bimodality due to an *in situ* halo forming through a quasi-monolithic collapse of enriched diffuse gas.

Comparison with other studies that describe *in situ* stellar haloes in hydrodynamical models of Milky Way-like galaxies suggests that a wide variety of physical mechanisms can be responsible for their formation. The relative importance of these processes is particularly sensitive to the implementation and resolution dependence of subgrid physical prescriptions for star formation and feedback. An improved understanding of these effects and observational constraints on star formation in free-floating gas clouds are thus necessary before definitive conclusions about *in situ* stellar halo formation can be drawn from any particular simulation. This uncertainty is currently the most important limitation on theoretical predictions for the *in situ* stellar halo. The comparison of simulations from different groups will be extremely useful in this regard, hence our emphasis on simple origin-based definitions for the different halo components.

ACKNOWLEDGEMENTS

The authors thank the anonymous referee for their insightful and constructive suggestions. They are grateful to Takashi Okamoto, who developed our simulation code, and Patricia Tissera, for useful discussions. APC is supported by a COFUND/Durham Junior Research Fellowship under EU grant [267209] and thanks Liang Gao for support in the early stages of this work under a CAS International Research Fellowship and NSFC grant [11350110323]. OHP was supported by NASA grant NNX10AH10G and by NSF grant CMMI1125285. CSF acknowledges an ERC Advanced Investigator grant COSMIWAY [GA 267291]. This work was supported by the Science and Technology Facilities Council [ST/L00075X/1] and used the DiRAC Data Centric system at Durham University, operated by the Institute for Computational Cosmology on behalf of the STFC DiRAC HPC Facility (`www.dirac.ac.uk`). This equipment was funded by BIS National E-infrastructure capital grant ST/K00042X/1, STFC capital grant ST/H008519/1, and STFC DiRAC Operations grant ST/K003267/1 and Durham University. DiRAC is part of the National E-Infrastructure.

REFERENCES

Abadi M. G., Navarro J. F., Steinmetz M., Eke V. R., 2003, ApJ, 591, 499
Aumer M., White S. D. M., 2013, MNRAS, 428, 1055
Aumer M., White S. D. M., Naab T., Scannapieco C., 2013, MNRAS, 434, 3142
Beers T. C. et al., 2012, ApJ, 746, 34
Bell E. F. et al., 2008, ApJ, 680, 295
Belokurov V. et al., 2006, ApJ, 642, L137
Bett P. E., Frenk C. S., 2012, MNRAS, 420, 3324
Binney J., Merrifield M., 1998, Galactic Astronomy. Princeton University Press, Princetion, NJ
Bovy J., Rix H.-W., Hogg D. W., 2012, ApJ, 751, 131
Brook C. B., Kawata D., Gibson B. K., Flynn C., 2004, MNRAS, 349, 52
Bullock J. S., Johnston K. V., 2005, ApJ, 635, 931
Carollo D. et al., 2010, ApJ, 712, 692
—, 2007, Nature, 450, 1020
Cooper A. P., Cole S., Frenk C. S., Helmi A., 2011, MNRAS, 417, 2206
Cooper A. P. et al., 2010, MNRAS, 406, 744
Crain R. A., McCarthy I. G., Frenk C. S., Theuns T., Schaye J., 2010, MNRAS, 407, 1403
Deason A. J., Belokurov V., Evans N. W., 2011, MNRAS, 416, 2903
DeBuhr J., Ma C.-P., White S. D. M., 2012, MNRAS, 426, 983
Dolag K., Borgani S., Murante G., Springel V., 2009, MNRAS, 399, 497
Font A. S., McCarthy I. G., Crain R. A., Theuns T., Schaye J., Wiersma R. P. C., Dalla Vecchia C., 2011, MNRAS, 416, 2802

Frenk C. S., Evrard A. E., White S. D. M., Summers F. J., 1996, ApJ, 472, 460
Fuchs B., Jahreiß H., 1998, A&A, 329, 81
Gilmore G., Reid N., 1983, MNRAS, 202, 1025
Gould A., Flynn C., Bahcall J. N., 1998, ApJ, 503, 798
Guedes J., Callegari S., Madau P., Mayer L., 2011, ApJ, 742, 76
Helmi A., Cooper A. P., White S. D. M., Cole S., Frenk C. S., Navarro J. F., 2011, ApJ, 733, L7
Hobbs A., Read J., Power C., Cole D., 2013, MNRAS, 434, 1849
Ivezić Ž., Beers T. C., Jurić M., 2012, ARA&A, 50, 251
Ivezić Ž. et al., 2008, ApJ, 684, 287
Kaufmann T., Mayer L., Wadsley J., Stadel J., Moore B., 2006, MNRAS, 370, 1612
Kazantzidis S., Bullock J. S., Zentner A. R., Kravtsov A. V., Moustakas L. A., 2008, ApJ, 688, 254
Kereš D., Vogelsberger M., Sijacki D., Springel V., Hernquist L., 2012, MNRAS, 425, 2027
McCarthy I. G., Font A. S., Crain R. A., Deason A. J., Schaye J., Theuns T., 2012, MNRAS, 420, 2245
McConnachie A. W. et al., 2009, Nature, 461, 66
McConnachie A. W., 2012, AJ, 144, 4
Maller A. H., Bullock J. S., 2004, MNRAS, 355, 694
Martínez-Delgado D. et al., 2010, AJ, 140, 962
Navarro J. F. et al., 2010, MNRAS, 402, 21
Okamoto T., 2013, MNRAS, 428, 718
Okamoto T., Frenk C. S., Jenkins A., Theuns T., 2010, MNRAS, 406, 208
Parry O. H., Eke V. R., Frenk C. S., Okamoto T., 2012, MNRAS, 419, 3304
Pillepich A., Madau P., Mayer L., 2015, ApJ, 799, 184
Price D. J., 2008, J. of Comput. Phys., 2271, 10040
Purcell C. W., Bullock J. S., Kazantzidis S., 2010, MNRAS, 404, 1711
Read J. I., Lake G., Agertz O., Debattista V. P., 2008, MNRAS, 389, 1041
Rix H.-W., Bovy J., 2013, A&A Rev., 21, 61
Ruchti et al. 2015, MNRAS, 450, 2874
Saitoh T. R., Makino J., 2009, ApJ, 697, L99
Sales L. V. et al., 2009, MNRAS, 400, L61
Sales L. V., Navarro J. F., Theuns T., Schaye J., White S. D. M., Frenk C. S., Crain R. A., Dalla Vecchia C., 2012, MNRAS, 423, 1544
Sandage A., Fouts G., 1987, AJ, 93, 74
Sawala T., Frenk C. S., Crain R. A., Jenkins A., Schaye J., Theuns T., Zavala J., 2013, MNRAS, 431, 1366
Scannapieco C. et al., 2012, MNRAS, 423, 1726
Schaye J. et al., 2015, MNRAS, 446, 521
Schlesinger K. J. et al., 2014, ApJ, 791, 112
Searle L., Zinn R., 1978, ApJ, 225, 357
Snyder G. F. et al., 2015, preprint (astro-ph/502.07747)
Springel V. et al., 2008, MNRAS, 391, 1685
Springel V., White S. D. M., Tormen G., Kauffmann G., 2001, MNRAS, 328, 726
Tissera P. B., Beers T. C., Carollo D., Scannapieco C., 2014, MNRAS, 439, 3128
Tissera P. B., Scannapieco C., Beers T. C., Carollo D., 2013, MNRAS, 432, 3391
Tissera P. B., White S. D. M., Scannapieco C., 2012, MNRAS, 420, 255
Wang J. et al., 2011, MNRAS, 413, 1373
White S. D. M., Frenk C. S., 1991, ApJ, 379, 52
White S. D. M., Rees M. J., 1978, MNRAS, 183, 341
Xue X.-X. et al., 2011, ApJ, 738, 79
Yoshii Y., 1982, PASJ, 34, 365
Zolotov A. et al., 2012, ApJ, 761, 71
Zolotov A., Willman B., Brooks A. M., Governato F., Brook C. B., Hogg D. W., Quinn T., Stinson G., 2009, ApJ, 702, 1058

APPENDIX A: QUANTITATIVE COMPARISON WITH TISSERA ET AL.

The initial conditions of haloes Aq-C and Aq-D have already been simulated by another group using different subgrid prescriptions and at slightly lower resolution, as reported by Tissera et al. (2012, 2013, 2014). This appendix provides a more detailed quantitative comparison of results for these two haloes to supplement the discussion in Section 7. Here we apply the definitions of components given by Tissera et al. to our simulations in place of the definitions in Section 3.

Briefly, in section 2.2 of T12, Tissera et al. define an *optical radius* $r_{\rm opt}$ enclosing 83 per cent of the total galaxy stellar mass. A *central* stellar component is defined by all stars with binding energy E less than $E_{\rm cen}$, the minimum binding energy of stars with $r > 0.5\,r_{\rm opt}$. Another threshold energy, $E_{\rm inner}$, is defined as the minimum binding energy of stars with $r > 2\,r_{\rm opt}$; stars with $E_{\rm cen} < E < E_{\rm inner}$ constitute the *inner halo* component, and stars with $E > E_{\rm inner}$ the *outer halo* component[2]. Stars with present-day circularity $\mathcal{E} > 0.65$ are assigned to the *disc* component, regardless of their binding energy. In the inner and outer halo components, stars that form within the virial radius of the main halo are classified as *disc heated* if they have $\mathcal{E} > 0.65$ in any output of the simulation. Since the disc is 'hotter' by definition in T12 than in our approach, relatively fewer disc stars will be classified as 'heated'. On the other hand, the heated disc category in T12 is not restricted to stars scattered from the $z = 0$ disc, which could counter the effect of a lower circularity threshold by increasing the number of stars assigned to this component[3].

Stars that are not heated disc are classified as *endo debris* if they form within the virial radius[4] and *debris* (which

[2] We find $r_{\rm opt}$ values similar to those of T12. The energy thresholds corresponding to the different components are only slightly different from those in fig. 1 of T12: we find $(E_{\rm cen}, E_{\rm inner}) = (-2.48, -1.56) \times 10^5$ and $(-1.78, -1.11) \times 10^5\,{\rm km^2 s^{-2}}$, for Aq-C and Aq-D respectively. If we impose the T12 values of $r_{\rm opt}$ we find $(E_{\rm cen}, E_{\rm inner}) = (-2.22, -1.33) \times 10^5$ and $(-1.90, -1.25) \times 10^5\,{\rm km^2 s^{-2}}$.

[3] Section 2.2 of T13 states that their classification, including the identification of the disc, is only applied at redshifts $z \lesssim 4$. The C15 results reported in Table A1 do not include this restriction. If we restrict the assignment of stars to the heated disc category to those formed at $z \lesssim 4$ (classifying those formed earlier as endo-debris), we find that the only significant change is to the inner halo heated disc component of Aq-C, reducing its mass fraction from 13 to 6 per cent.

[4] In our implementation of these definitions, membership of the self-bound halo identified by `SUBFIND` is used as a proxy for a particle being 'within the virial radius'.

we call *accreted*) otherwise. Importantly, the endo-debris class includes stars that form bound to satellites within the virial radius which are later stripped – in the main text we classify these as accreted rather than *in situ*.

Table A1 compares the masses and mass fractions of various components between the two subgrid implementations and Fig. A1 shows the density profiles of the different components. Differences in the properties of the stellar halo need to be interpreted in the context of large differences in the bulk properties of the central galaxies (summarized in Scannapieco et al. 2012). Relative to T12, our galaxies convert about 50 per cent less of their total baryonic mass to stars overall[5] but still have more massive discs (by factors of 6.5 for Aq-C and 1.5 for Aq-D). The central ('bulge') component is less massive in our simulations (by 49 and 28 per cent respectively). The inner halo component differs even more – roughly a factor of 10 less massive in our Aq-C and a factor of 6 less massive in our Aq-D. The outer halo is most closely comparable, being only slightly less massive in our simulations.

Given these differences, it is more useful to compare mass fractions than absolute masses. In the Tissera et al. inner halo component, we find a substantially smaller contribution from scattered disc stars (discussed in the main text) and a much larger contribution from endo-debris. The balance between *in situ* and accreted stars is slightly in favour of the former in our simulations thanks to this larger endo-debris contribution and a much lower mass of accreted stars in the same region. As shown in Fig. A1, most of the endo-debris in our simulation comes from star formation in galaxies after they have become satellites. In the outer halo, the masses of endo-debris stars in our simulations are similar to those reported by Tissera et al., but the accreted stellar mass in this region is roughly two to three times lower, giving a higher endo-debris fraction. Since endo-debris stars formed in satellites constitute the majority of endo-debris outside ~ 30 kpc in our simulations, it is not surprising that the endo debris and debris (accreted) profiles in Fig. A1 are very similar.

We conclude that the star formation model in our simulations results in satellites that are more gas rich at accretion and that form stars more vigorously thereafter, leading, in the language of Tissera et al., to more endo-debris and less debris. This is consistent with star formation overall being more efficient in the Tissera et al. simulations.

It is interesting in this regard that our simulations and those of Tissera et al. are consistent with the Milky Way satellite luminosity function, although this comparison involves only a small number of objects. The gas content of surviving satellites and dwarf galaxies outside the virial radius also provides a useful constraint on predictions for the formation of *in situ* from accreted gas. In our simulations, we examine the ratio of neutral ($T \lesssim 10^4$K) gas mass to stellar mass. We find 3, 8 and 9 satellites at $r < 250\,$kpc with $M_{\rm H_I}/M_\star > 1\times10^{-4}$ in haloes C, D and E respectively, only slightly in excess of the same count around the Milky Way (4) and M31 (5, including M33). Outside this radius, we find that our simulated dwarf galaxies have a median gas fraction of $M_{\rm H_I}/M_\star \sim 10$, considerably higher than the observed median for the Local Group, $M_{\rm H_I}/M_\star \sim 1$ (McConnachie 2012). This supports the idea that, in our models, a low star formation efficiency before infall may lead to high star formation rates in stripped gas and in recently accreted satellites.

As noted in the main text, the high star efficiency of the central galactic spheroid, presumably fuelled by smoothly accreted gas, might also explain the substantially lower metallicity of the endo-debris component in T13. Another point worthy of note is that our simulations predict even lower halo stellar mass from disc heating than Tissera et al., despite producing more massive discs at $z = 0$.

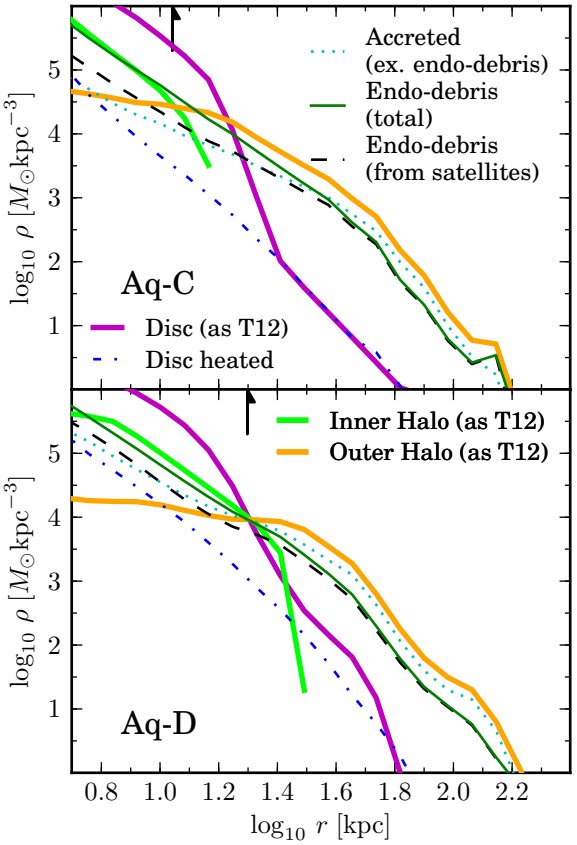

Figure A1. Density profiles of stellar components in our simulations Aq-C and Aq-D according to the definitions of T12 and T13 (see the text). Thin lines show different categories of halo stars – accreted (dotted; called debris by T13), endo-debris (solid) and heated disc (dot–dashed). In addition we show separately the profile of stars that meet the T13 definition of endo-debris but which we would classify as accreted, because they form bound to satellites (long dashed). Thick lines show profiles of all stars in different phase space 'regions' – disc, inner and outer haloes. Arrows mark the radius $r_{\rm opt}$ defined by T12. The 'central' component of T13 is confined to $\log_{10} r/{\rm kpc} < 0.8$ and hence is not shown.

APPENDIX B: NUMERICAL RESOLUTION

We have reported three mechanisms responsible for the generation of *in situ* halo stars in our simulations – disc heating, star formation in stripped gas and star formation in

[5] Our simulations would convert slightly more baryons into stars at the lower resolution of T12 – see appendix B.

Table A1. Columns compare results for haloes Aq-C and Aq-D as simulated by Tissera et al. (2012, 2013; T12, T13) and in this work (C15), using the definitions given in T12 and T13 in all cases. The first row gives the optical radius defined by T12 as enclosing a stellar mass $M_{\star,\rm opt}$ (second row) equal to 83 per cent of the total stellar mass of the galaxy, $M_\star$. Rows 3 to 7 give the mass of stars in different galactic components of T12, described in the text. Rows 8 to 13 separate the inner halo component by origin according to T13, giving the mass of 'debris', 'heated disc' and 'endo–debris' stars and their relative fractions. Rows 14–19 give the same breakdown for the outer halo component. All quantities assume $h = 0.73$.

		Aq-C		Aq-D	
		T12	C15	T12	C15
$r_{\rm opt}$	[kpc]	16.0	11.0	14.8	19.8
$M_{\star,\rm opt}$	$[10^9 {\rm M}_\odot]$	8.12	3.49	6.04	2.86
$M_{\rm disc}$	$(10^9 {\rm M}_\odot]$	2.19	14.3	12.2	18.3
$M_{\rm central}$	$(10^9 {\rm M}_\odot]$	51.8	22.7	32.9	9.37
$M_{\rm inner}$	$(10^9 {\rm M}_\odot]$	19.5	1.99	18.6	2.94
$M_{\rm outer}$	$(10^9 {\rm M}_\odot]$	4.93	3.02	5.48	3.87
$M_{\rm total}$	$(10^9 {\rm M}_\odot]$	78.4	42.0	69.2	34.5
Inner Halo					
$M_{\rm debris}$	$(10^9 {\rm M}_\odot]$	8.58	0.19	8.00	0.90
$M_{\rm heated}$	$(10^9 {\rm M}_\odot]$	4.68	0.27	4.84	0.39
$M_{\rm endo}$	$(10^9 {\rm M}_\odot]$	6.24	1.53	5.58	1.65
$f_{\rm debris}$	%	44	9	43	31
$f_{\rm heated}$	%	24	13	26	13
$f_{\rm endo}$	%	32	77	30	56
Outer Halo					
$M_{\rm debris}$	$(10^9 {\rm M}_\odot)$	3.90	1.35	4.16	2.34
$M_{\rm heated}$	$(10^9 {\rm M}_\odot)$	0.00	0.06	0.00	0.07
$M_{\rm endo}$	$(10^9 {\rm M}_\odot)$	1.04	1.62	1.31	1.47
$f_{\rm debris}$	%	79	45	76	60
$f_{\rm heated}$	%	0	2	0	2
$f_{\rm endo}$	%	21	53	24	38

smoothly accreted gas – and discussed similarities and differences with other simulations at comparable resolution. All three mechanisms are all likely to be sensitive to numerical resolution, for different reasons.

The disc heating dynamics in N-body simulations and their resolution dependence have been studied extensively (e.g. Kazantzidis et al. 2008; Read et al. 2008; Purcell et al. 2010); in ab initio simulations there is an additional dependence on the subgrid physics governing the formation and structure of the disc (e.g DeBuhr et al. 2012; Aumer et al. 2013). This dependence is now being tackled directly, with some success, by recent generations of hydrodynamical simulations (Scannapieco et al. 2012; Aumer & White 2013; Schaye et al. 2015; Snyder et al. 2015). The behaviour of subgrid star formation models is less well understood in the regime of dwarf galaxies, where there are fewer constraints – the most important being comparison to the satellite luminosity functions of the Milky Way and M31 (e.g. Parry et al. 2012; Zolotov et al. 2012; Sawala et al. 2013). The star formation histories of satellites determine their contribution to the accreted halo and their gas content at accretion, which provides the reservoir for star formation in tidal and ram-pressure streams. The formation of stars in gaseous streams and clumps depends on the treatment of hydrodynamic interactions within circumgalactic haloes of hot gas (e.g. Maller & Bullock 2004). Moreover, although these hot gas haloes are a robust prediction of the CDM model, their detailed properties in simulations are known to be sensitive to the treatment of thermal instabilities and galactic winds (and, potentially, active galactic nuclei). Subgrid star formation models are typically calibrated in the context of a dense cold ISM, with star formation in unstable pockets of halo gas most often considered a 'nuisance' effect (e.g. Kaufmann et al. 2006; Kereš et al. 2012; Parry et al. 2012; Hobbs et al. 2013).

Since our main purpose is to present the phenomenology of particular sets of hydrodynamical simulations, rather than make predictions for specific observations, we have not carried out detailed convergence studies to address these issues. It is possible that the numerical effects given above are dominant over physical behaviour in all cases; hence, tests of convergence will be absolutely essential for any robust predictive model of *in situ* stellar halo formation.

In this respect we believe the formation of stars from 'smoothly accreted' hot gas to be the least robust of the mechanisms we identify, having three likely sources of resolution dependence: the behaviour of the subgrid star formation model, the treatment of thermal instabilities and the classification of particles as 'smoothly' accreted. It is not at all clear a priori which of these dependences is most important for convergence.

In Fig. B1 we illustrate the resolution dependence of the density profile of stars formed from gas accreted smoothly by the main halo. The solid red line corresponds to Aq-C at our default resolution level (level 4), including the disc and the stellar halo. Solid lines of lighter colours correspond to simulations from the same initial conditions with progressively lower resolution (levels 5, particle mass $m_{\rm p} = 2.11 \times 10^6$, and 6, $m_{\rm p} = 1.69 \times 10^7$; these simulations are also discussed in Parry et al. 2012).

As resolution increases (from L6 to L4), the mass of stars formed from smoothly accreted gas is reduced at all radii. Although the profile of disc stars associated with this component appears to converge at resolution L5, this is not the case for the stellar halo. In a region $r > 30\,{\rm kpc}$, we find $4 \times 10^8 {\rm M}_\odot$ of stars formed from smoothly accreted gas at L6, representing 11 per cent of the stellar mass and 0.4 per cent of all baryons in the same region. With increasing resolution, we see a reduction in the total mass of this component by ~ 50 per cent for each level, a similar change in its mass relative to all stars (from 11 to 4 per cent, a 43 per cent reduction in this fraction per level) and a somewhat smaller reduction in its mass relative to all baryons (17 per cent in this fraction per level). Dashed lines in Fig. B1 tell a similar story for the gas that is smoothly accreted but not converted to stars – this is always the dominant baryonic mass component at $r > 30\,{\rm kpc}$.

The absolute change in the mass of halo stars formed from smoothly accreted gas is explained only in part by a reduction in the total baryonic mass of the halo by ~ 30 per cent from L6 to L4 (~ 36 per cent for $r > 30\,{\rm kpc}$; this can be compared to a 6 per cent decrease in total mass bound to the main substructure). Another significant factor must therefore be that the classification of a gas particle as 'smoothly accreted' may also not be converged, because gas

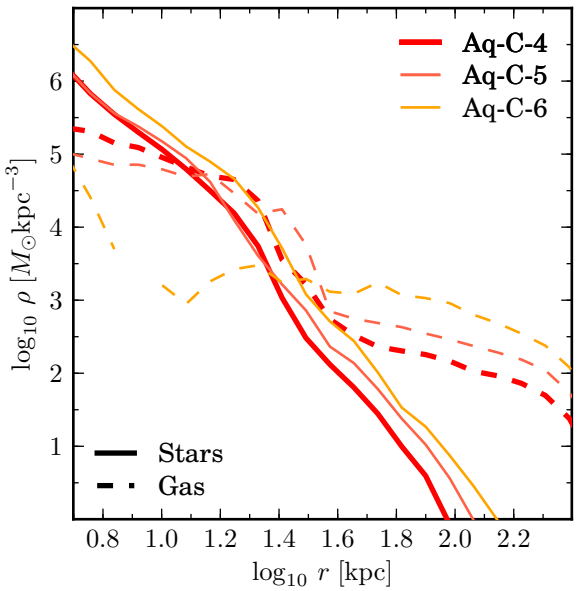

Figure B1. Present-day mass density profiles of smoothly-accreted gas particles (dashed) and all star particles formed from smoothly accreted gas (solid), in halo Aq-C at our default resolution level (L4). Thinner lines correspond to lower resolution levels L5 and L6 as described in the text.

associated with DM substructures resolved only at higher resolution will be classified as 'smoothly' accreted at lower resolution. This is illustrated by the results of Wang et al. (2011), who examine the total mass (baryons and DM) accreted smoothly on to the main halo in collisionless versions of the same initial conditions we simulate. Their fig. 9 shows a decrease of $\sim$ 13–15 per cent in the faction of 'smooth' accretion from L5 to L4 (depending on how 'smooth' accretion is defined). If all DM subhaloes supplied baryons to the main halo in the universal ratio, we would expect a similar reduction in the fraction of gas classified as smoothly accreted.

We conclude that, at lower resolution, more baryons are retained by the main halo and relatively more of these baryons are considered as smoothly accreted. The overall efficiency with which smoothly accreted gas is converted to stars also varies systematically with resolution, although (in our simulations) this is a minor contribution to the change of *in situ* stellar halo mass, relative to the first two effects.